Supporting Information

Graphene-Based Gas Sensors with High Sensitivity and Minimal Sensor-to-Sensor Variation

Jae Hong Choi,[a,1] Junghyun Lee,[b,1] Mirang Byeon,[c] Tae Eun Hong,[d] Hyesung Park,[*b] and Chang Young Lee[*a]

[a]Department of Chemical Engineering, School of Energy and Chemical Engineering, Ulsan National Institute of Science and Technology (UNIST), Ulsan 44919, Republic of Korea.

[b]Department of Energy Engineering, School of Energy and Chemical Engineering, Low Dimensional Carbon Materials Center, Perovtronics Research Center, Ulsan National Institute of Science and Technology (UNIST), Ulsan 44919, Republic of Korea.

[c]Busan Center, Korea Basic Science Institute, Busan 46742, Republic of Korea

[d]Center for Research Equipment, Korea Basic Science Institute, Busan 46742, Republic of Korea

[1]These authors contributed equally to this work.

Corresponding Authors

* Email: hspark@unist.ac.kr, cylee@unist.ac.kr

This PDF file includes Supporting Table S1-S2 and Figure S1-S23.

Table S1. Comparison of the Four Types of Graphene Sensors Obtained from 45 Sensors for Each Type

Preparation process	Before additional heat treatment		After additional heat treatment	
	$\Delta R/R_0$ (%)	S/N	$\Delta R/R_0$ (%)	S/N
Carbon o, annealing	0.13 ± 1.1	1.6 ± 2.2	-0.47 ± 0.19	85 ± 67
Carbon o, acetone	-0.03 ± 0.06	9.6 ± 26	-0.78 ± 0.13	360 ± 240
Carbon x, annealing	-0.15 ± 0.06	72 ± 57	-0.56 ± 0.05	310 ± 94
Carbon x, acetone	-0.01 ± 0.05	2.7 ± 8.7	-0.41 ± 0.14	54 ± 35

Table S2. Responses of Various Nanomaterials-Based Gas Sensors upon Exposure to DMMP Vapor

Materials	Detection range (ppm)	Response (%)	Ref.
Graphene	0.1 ~ 5	0.18 ~ 0.98	This study
PPy/Graphene	5 ~ 25	4.5 ~ 14.3	1
Triphenylene/Graphene	1.3	10	2
CuO/ZnO	10	626	3
rGO	1 ~ 50	2.1 ~ 9.0	4
rGO	10 ~ 40	24 ~ 77	5
CNTs	5 ~ 80	1.8 ~ 5.9	6
CNTs	25 ~ 50	5 ~ 8	7
CNTs	1 ~ 40	3.8 ~ 12.4	8
TFQ/CNTs	2×10^{-5} ~ 16	3.4 ~ 61	9
HFIPP/CNTs	0.05 ~ 0.2	0.3 ~ 1	10
HFIP-PT/CNTs	0.05 ~ 0.6	1 ~ 8	11
ZnO or SnO_2/CNTs	1×10^{-4} ~ 1	0.58 ~ 4.4	12

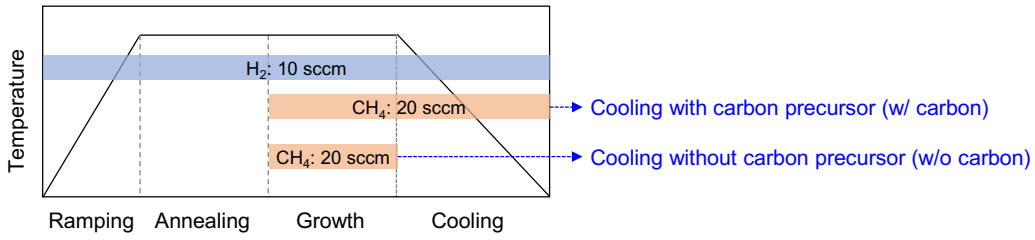

Fig. S1. CVD synthesis process, showing two different conditions depending on the presence of a carbon precursor.

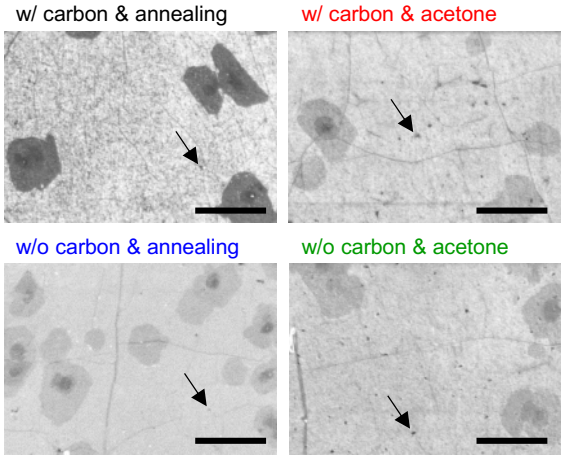

Fig. S2. SEM images of four types of graphene. Arrows indicate PMMA residues present in every type of graphene. Scale bars, 3 μm.

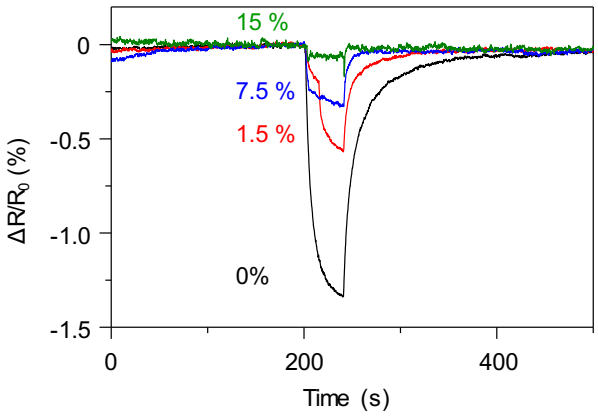

Fig. S3. Responses to 5 ppm DMMP at different relative humidity, showing reduced sensitivity under humid conditions.

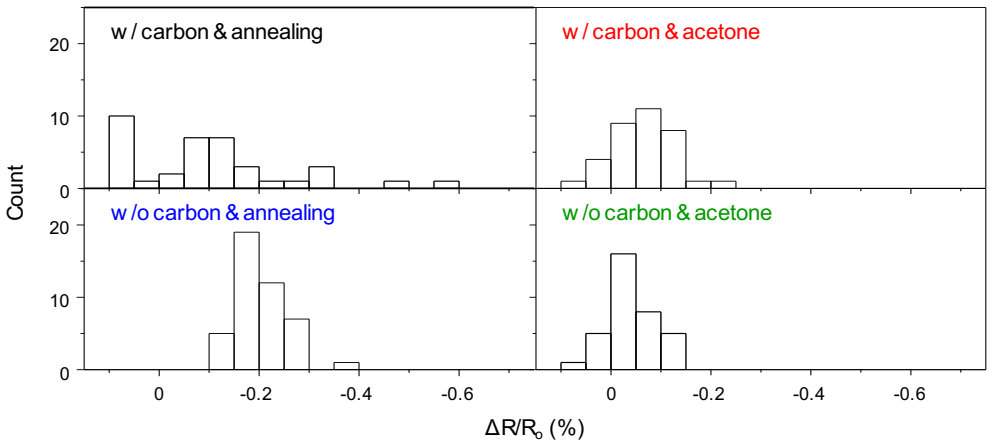

Fig. S4. Histograms showing sensor responses of four types of as-prepared graphene (before the additional heat treatment in air) upon exposure to 5 ppm DMMP. Each histogram is collected from 35 sensors.

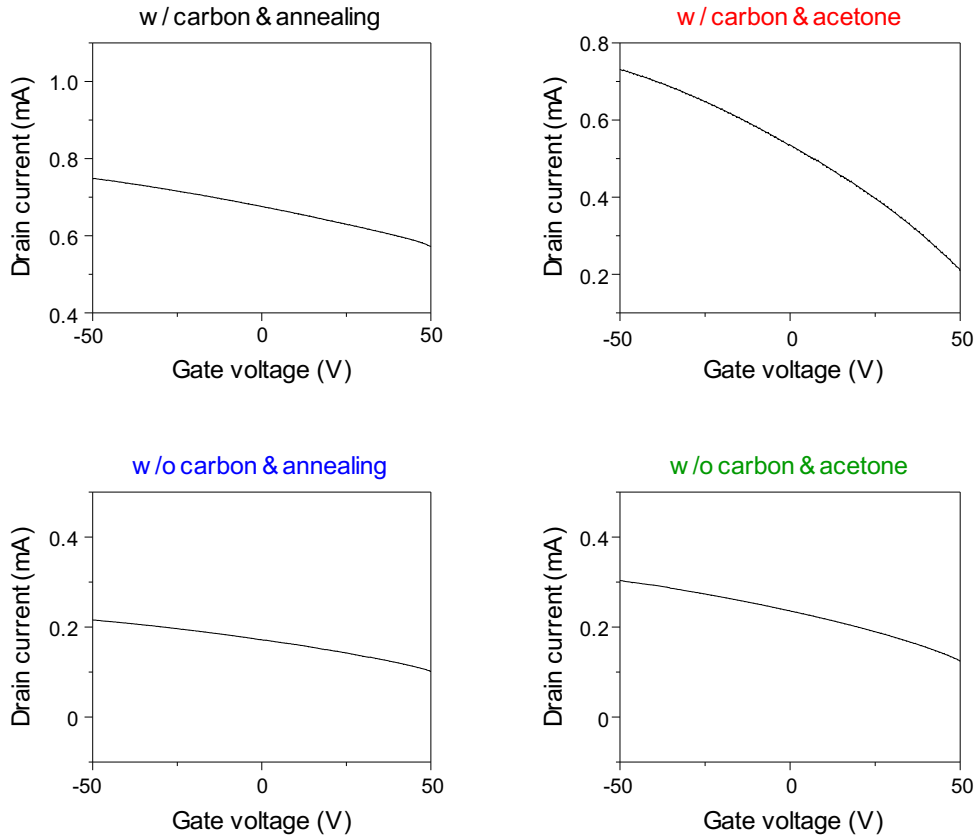

Fig. S5. Transfer characteristics of the four types of graphene sensors.

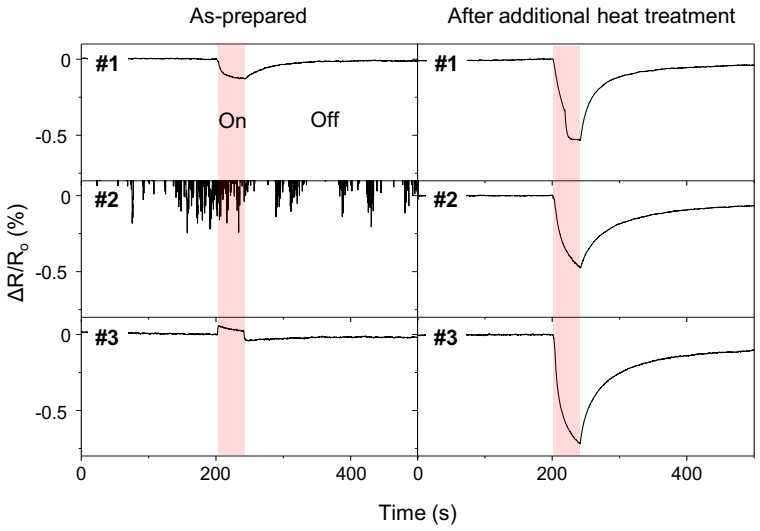

Fig. S6. Sensor responses to 5 ppm DMMP before (as-prepared) and after additional heat treatment in air. Three sensors, labeled #1 through #3, are used before and after the treatment. Sensor #1 shows enhanced response after the heat treatment. Sensor #2 shows high noise intensity and no response initially, but after the treatment both the noise and the signal are greatly improved. Sensor #3 shows a positive response to DMMP before annealing, but the direction turns negative after the heat treatment.

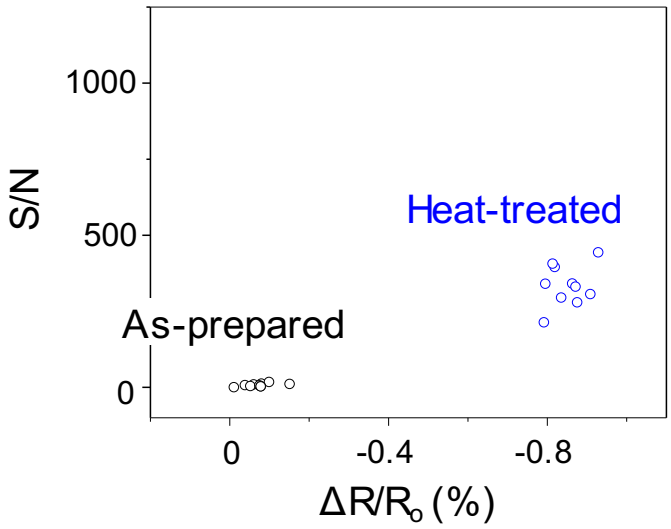

Fig. S7. Distribution of responses and S/N from the w/o carbon and annealing graphene. Before additional heat treatment in air (black), the sensors show poor responses to 5 ppm DMMP ($\Delta R/R_o = -0.15 \pm 0.06\%$). After additional heat treatment in air (blue), the responses are highly enhanced ($\Delta R/R_o = -0.85 \pm 0.05\%$).

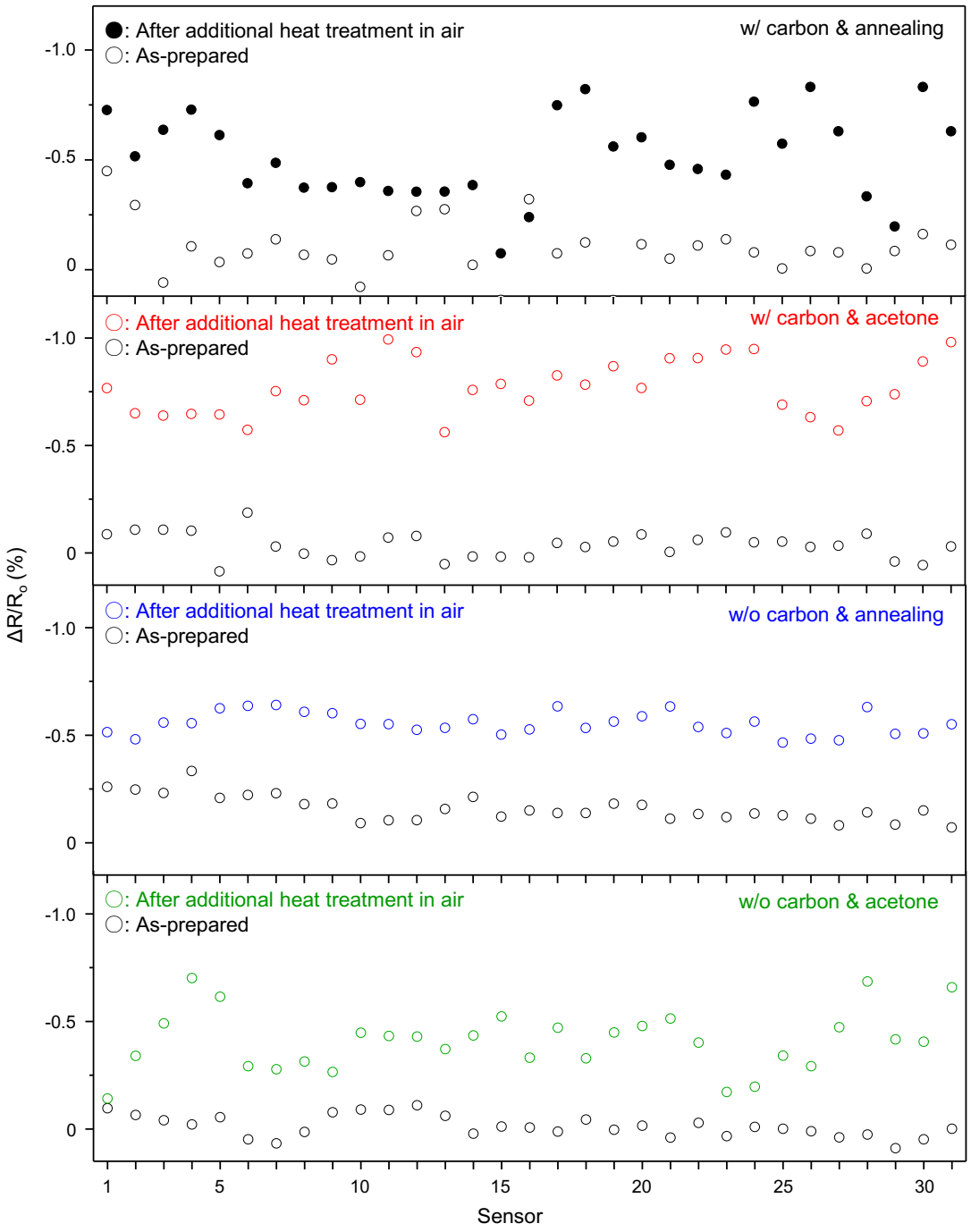

Fig. S8. Response from the same sensors before (as-prepared) and after additional heat treatment in air. The enhanced responses are observed in most sensors regardless of the type of graphene, but the w/o carbon & annealing graphene sensors show the most uniform responses.

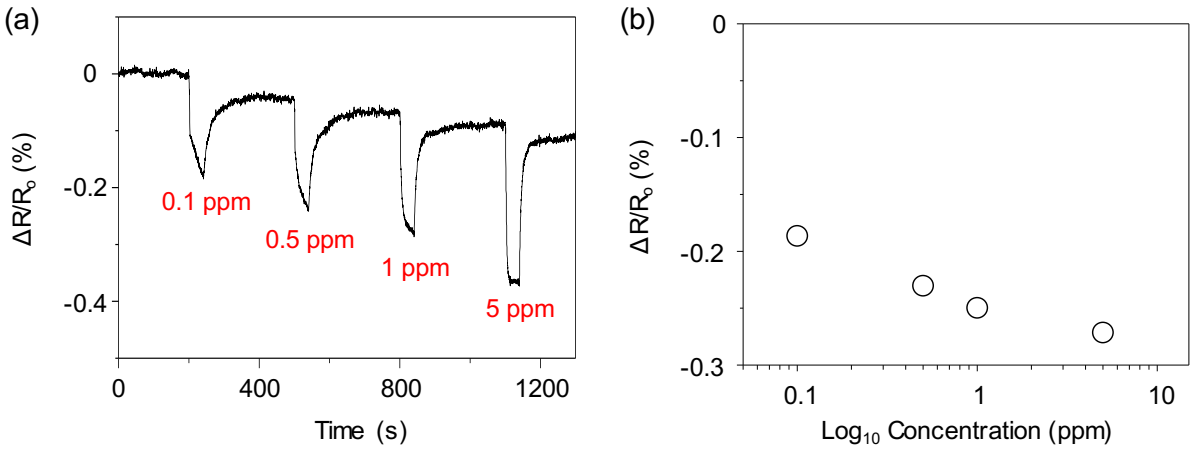

Fig. S9. Responses to DMMP vapor at different concentrations. (a) Response ($\Delta R/R_o$) vs. time at different DMMP concentrations. (b) A response curve to DMMP vapor, giving limit of detection (LOD) of 5 ppb at S/N of 3.

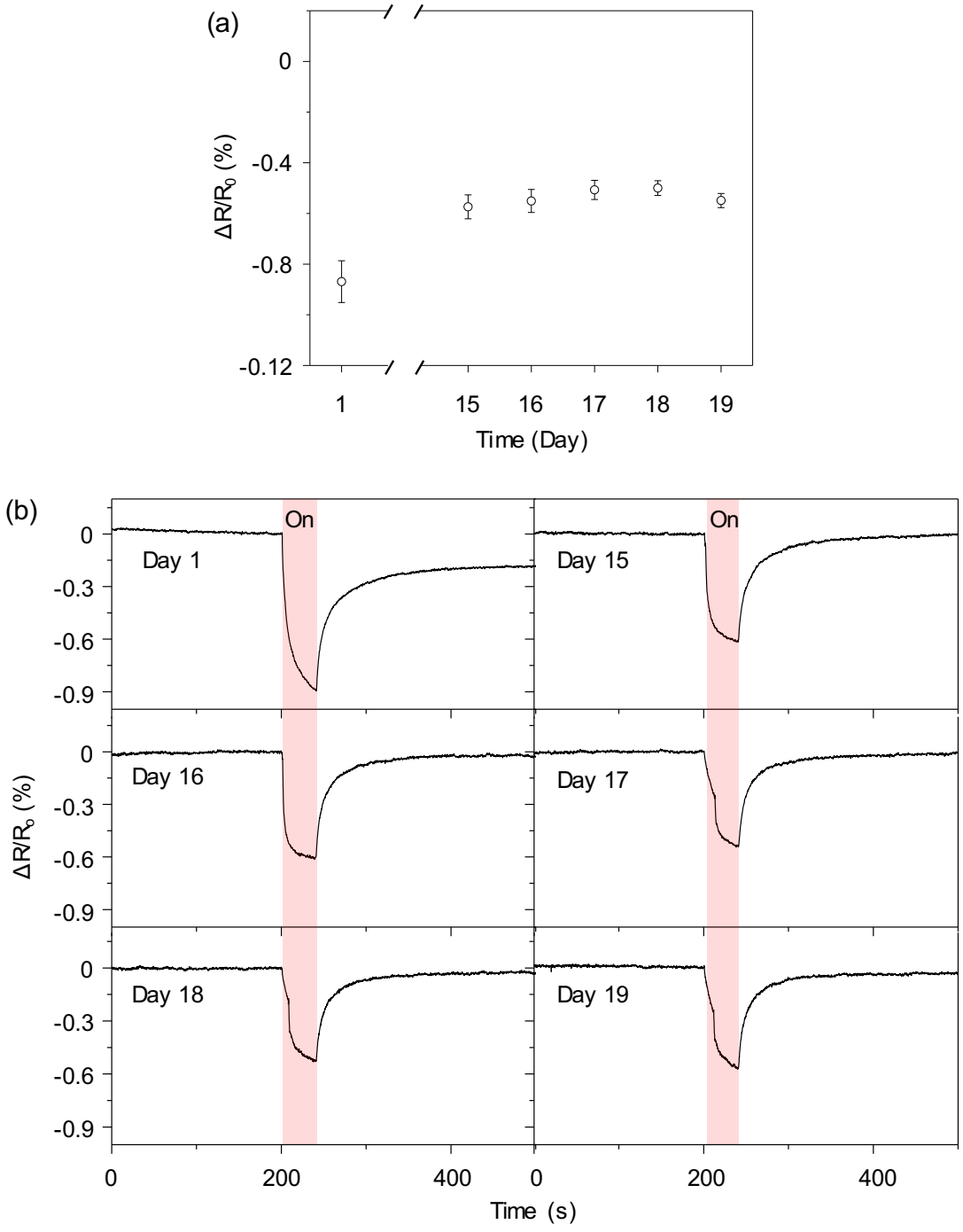

Fig. S10. Long-term stability of graphene-based gas sensors. (a) Response ($\Delta R/R_o$) to 5 ppm DMMP over a period of 19 days. The sensitivity is reduced by 35% after Day 1 and remains stable thereafter. (b) Representative sensor responses to 5 ppm DMMP over time. The response on Day 1 is partially irreversible, which explains the reduced sensitivity from Day 15.

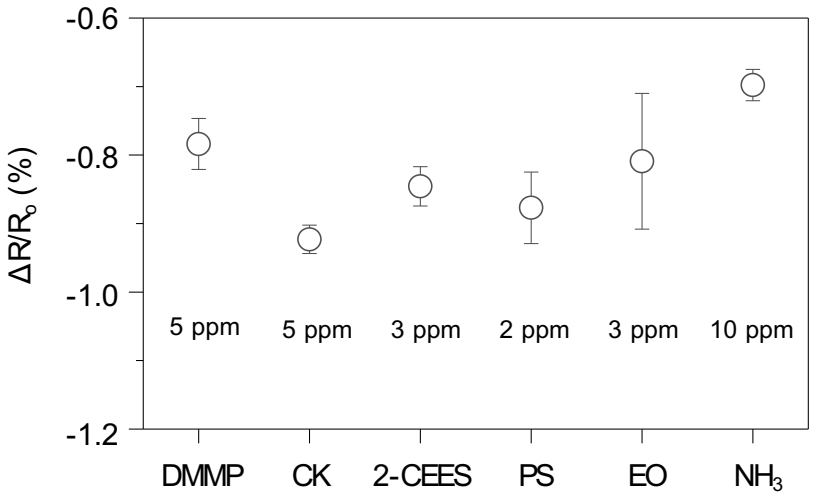

Fig. S11. Detection of various analytes using graphene-based gas sensors prepared w/o carbon & annealing. The sensors went through the additional heat treatment in air. Resistance change is shown upon exposure to DMMP, cyanogen chloride (CK), 2-chloroethyl ethyl sulfide (2-CEES), chloropicrin (PS), ethylene oxide (EO), and ammonia at the concentrations noted. Except for ethylene oxide, which showed a resistance change of 0.81±0.1%, the sensor responses are uniform with standard deviation below 0.05%. The selectivity is poor but can be improved by employing surface chemistry in other studies.

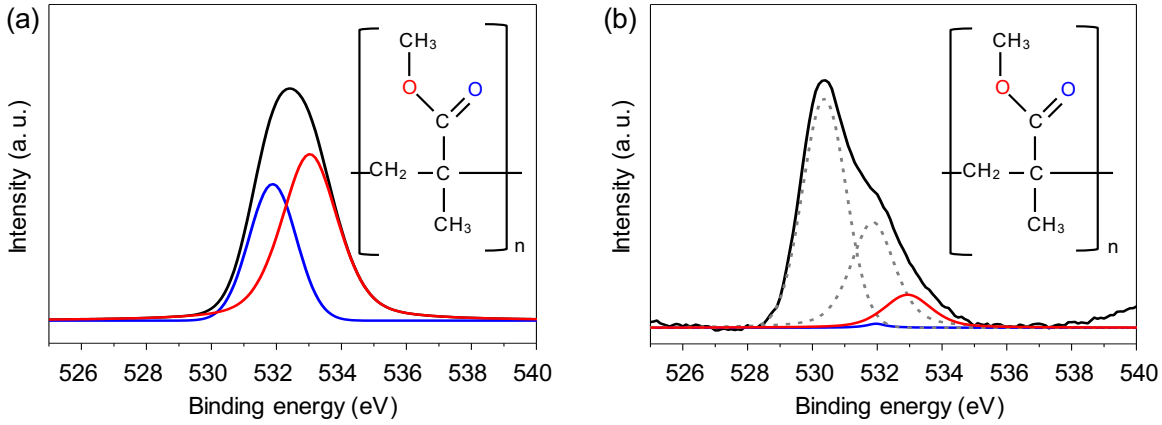

Fig. S12. Effect of additional heat treatment on O 1s XPS spectra of graphene on Au (50nm)-Ti (10nm)-Si substrate. (a) XPS spectra of as-prepared graphene (w/ carbon & acetone), showing two peaks identified as C=O (531.8 eV) and C-O (533.0 eV) from PMMA film.1 (b) XPS spectra of graphene after additional heat treatment in air at 300 °C for 1hr, showing sharply decreased peaks from C=O (531.8 eV, blue) and C-O (533.0 eV, red), which indicates incomplete removal of PMMA even by the additional heat treatment. The dotted peaks at 530.4 eV and 532.0 eV are from Au-O and water molecules adsorbed on Au, respectively.[13-17]

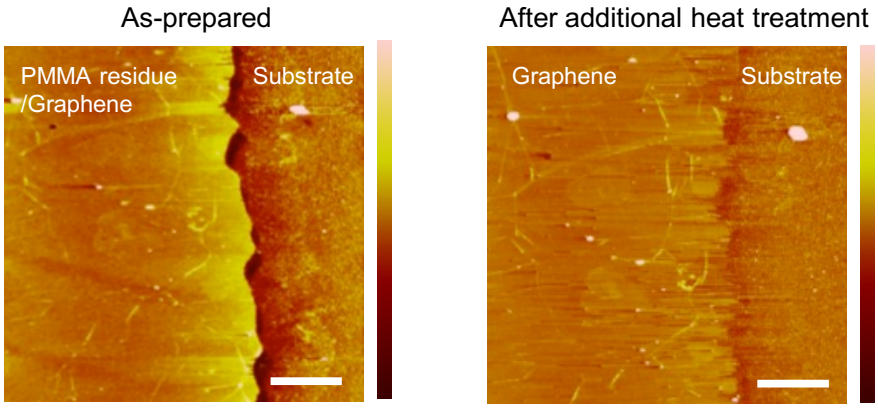

Fig. S13. AFM images of graphene/substrate interface before (as-prepared, w/ carbon & acetone) and after additional heat treatment in air. The graphene was annealed in air for 90 min at 300 ℃, and the AFM images before and after the treatment were obtained from exactly the same area. The thickness of the graphene is clearly reduced after annealing in air, indicating removal of PMMA residues. Scale bars, 2 μm. Color scale, 20 nm.

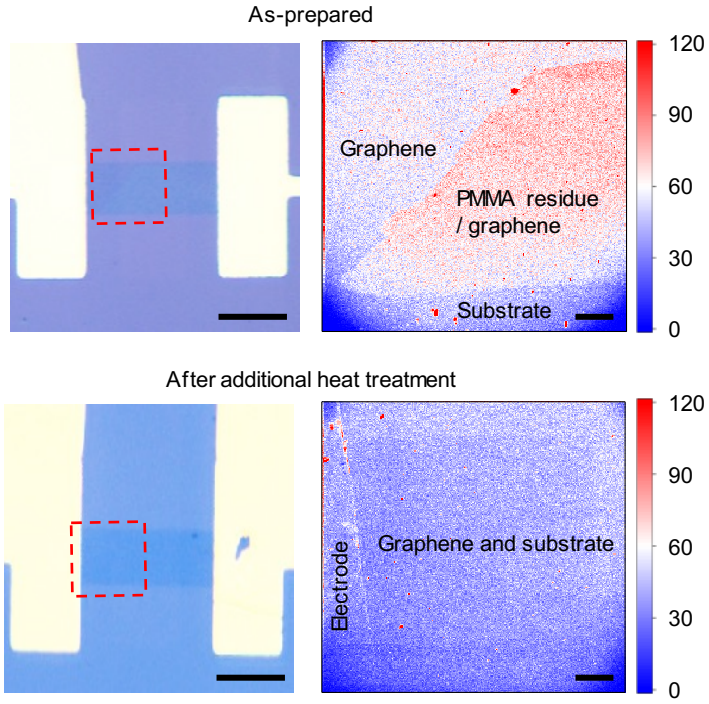

Fig. S14. Hydrogen distribution of PMMA residue before and after annealing in air. The surface elemental analysis of ^{1}H (right) were performed in the red dotted area in the optical images (left). In the as-prepared graphene (w/ carbon & acetone), the ^{1}H signal of PMMA residues was strong from the lower right region of the mapped area. However, the ^{1}H signal disappeared after additional heat treatment in air, suggesting removal of PMMA residues from the graphene surface. Scale bars, 100 μm in optical images (left) and 10 μm in Nano-SIMS images (right).

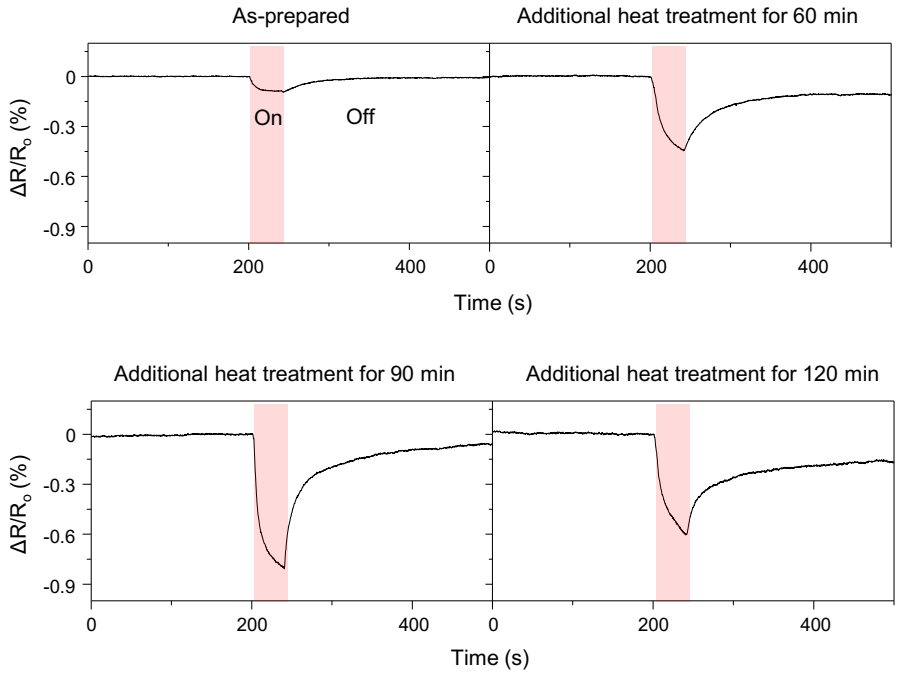

Fig. S15. Enhanced responses after additional heat treatment in air. The response to 5 ppm DMMP is small in as-prepared sensor, enhanced after 60 min heat treatment, further enhanced after 90 min treatment, and then decreased after 120 min treatment.

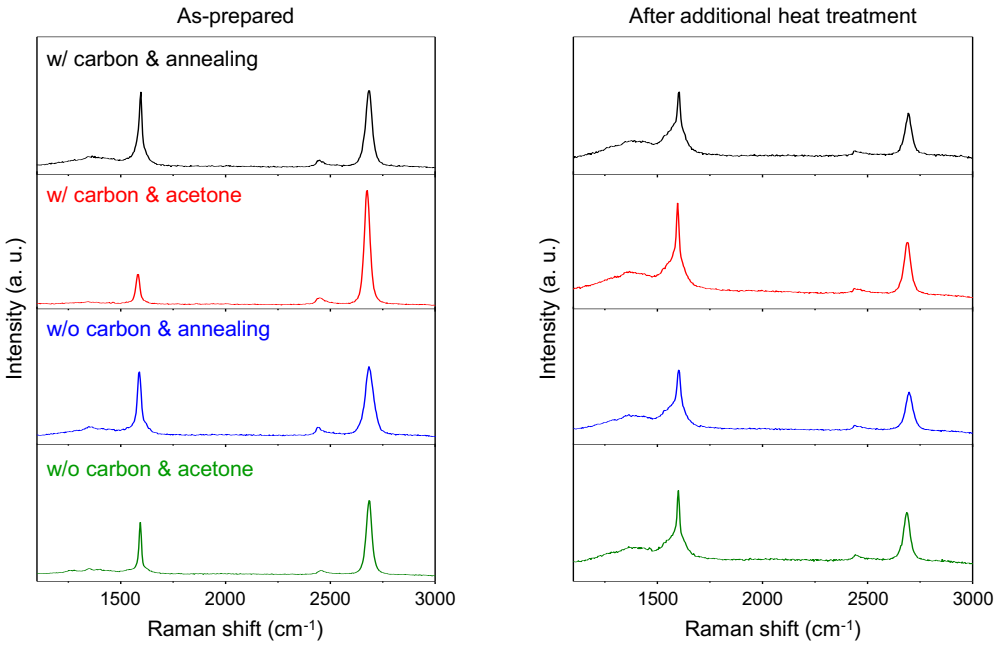

Fig. S16. Raman spectra of four types of graphene before (as-prepared) and after additional heat treatment in air for 90 min. Although all the graphenes are single layer, the I_{2D}/I_G ratio of w/ carbon & annealing graphene and w/o carbon & annealing graphene are ~ 1 because of oxygen doping. The w/ carbon & acetone graphene shows an I_{2D}/I_G ratio of >2, which indicate the highest quality graphene among the four types of graphene. After annealing in air, the intensity of 2D peak decreases and the background of the D-mode increases.

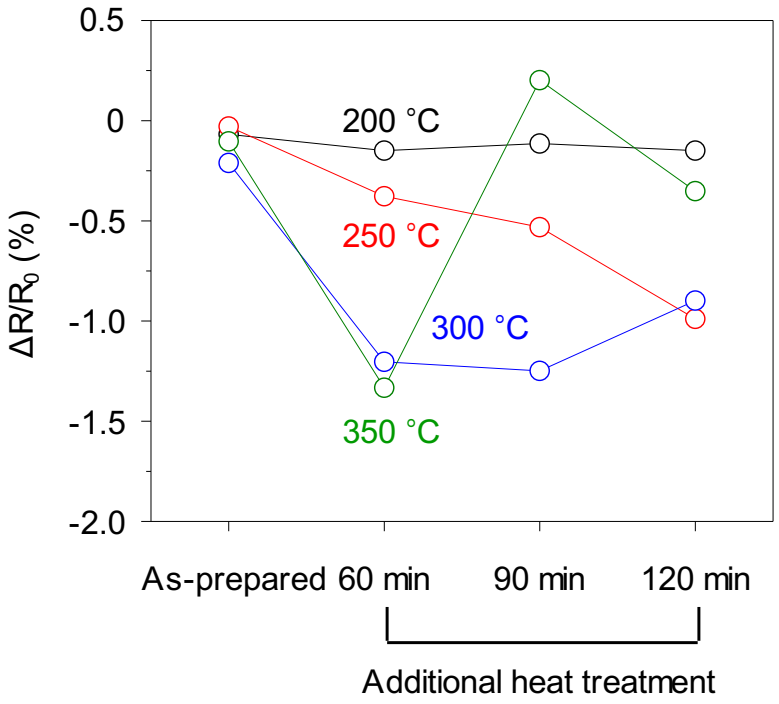

Fig. S17. The effect of annealing temperature and time on the sensor responses. At 200 ℃, the effect of annealing on the sensor response is negligible, whereas at 250 ℃ the response keeps increasing as the annealing time increases. Annealing at 300 ℃ improves the response after 60 min and remains stable even after longer heat treatment. At 350 ℃, however, the improved response at 60 min sharply decreases after 90 min, suggesting potential damage in the graphene. Therefore, we found 300 ℃ to be an optimal temperature for the additional heat treatment.

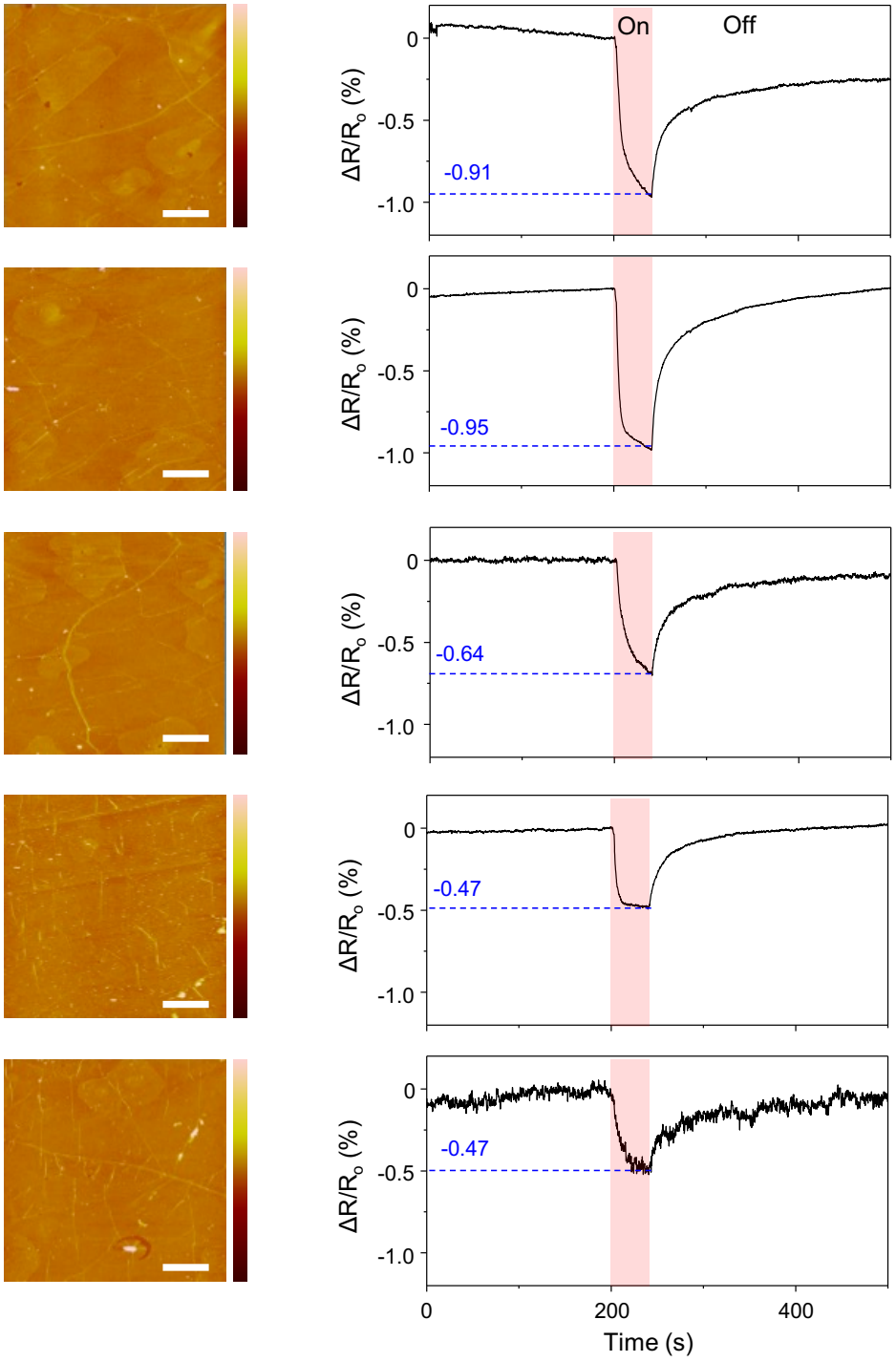

Fig. S18. AFM images of w/ carbon & acetone graphene, with corresponding sensor responses to 5 ppm DMMP shown on the right. There is a large sensor-to-sensor variation in responses. The sensitivity decreases as the amount of wrinkles and PMMA residues increase from top to bottom. Scale bars, 2 μm. Color scale, 20 nm.

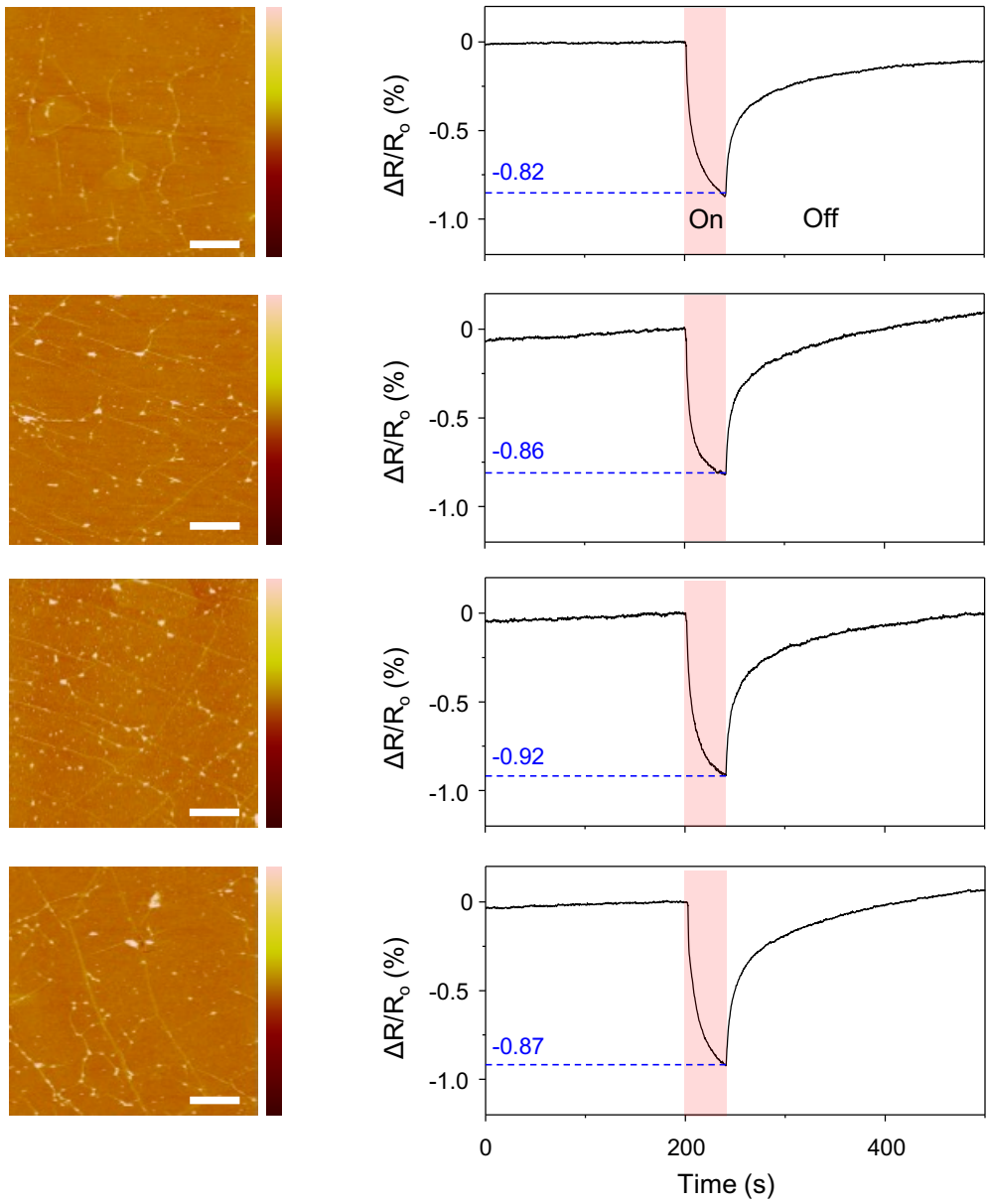

Fig. S19. AFM images of w/o carbon & annealing graphene, with corresponding sensor responses to 5 ppm DMMP shown on the right. The surface is not as clean as the w/ carbon and acetone graphene, but the degree of wrinkles and PMMA residues is uniform in different sensors, resulting in uniform sensor responses. Scale bars, 2 μm. Color scale, 20 nm.

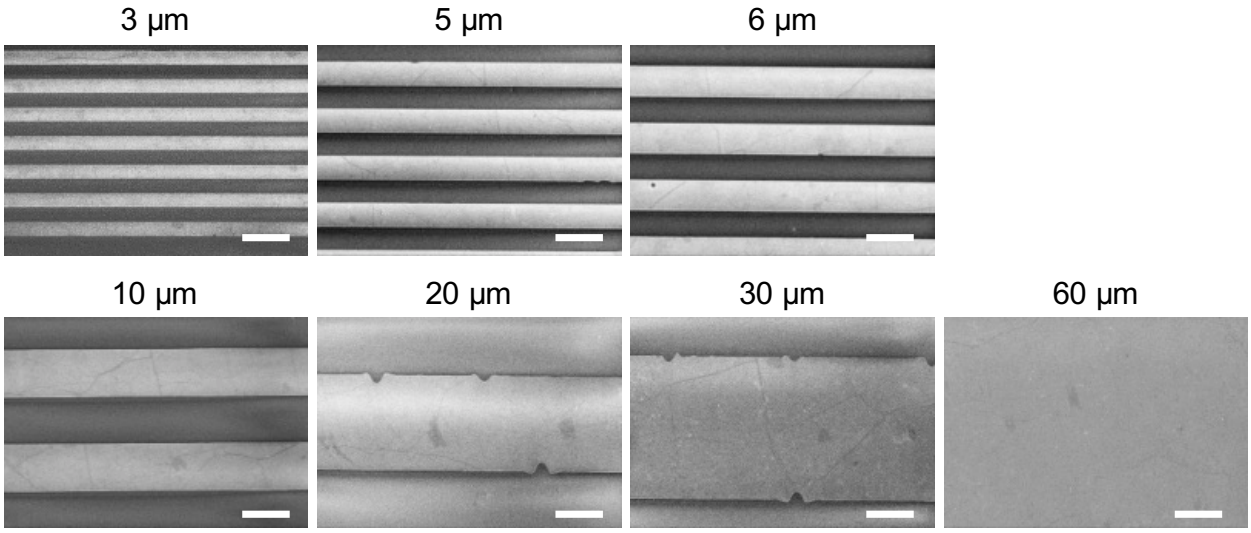

Fig. S20. SEM images of graphene with different edge-to-surface ratio, supporting that the graphene is mostly a single layer. Scale bars, 10 µm.

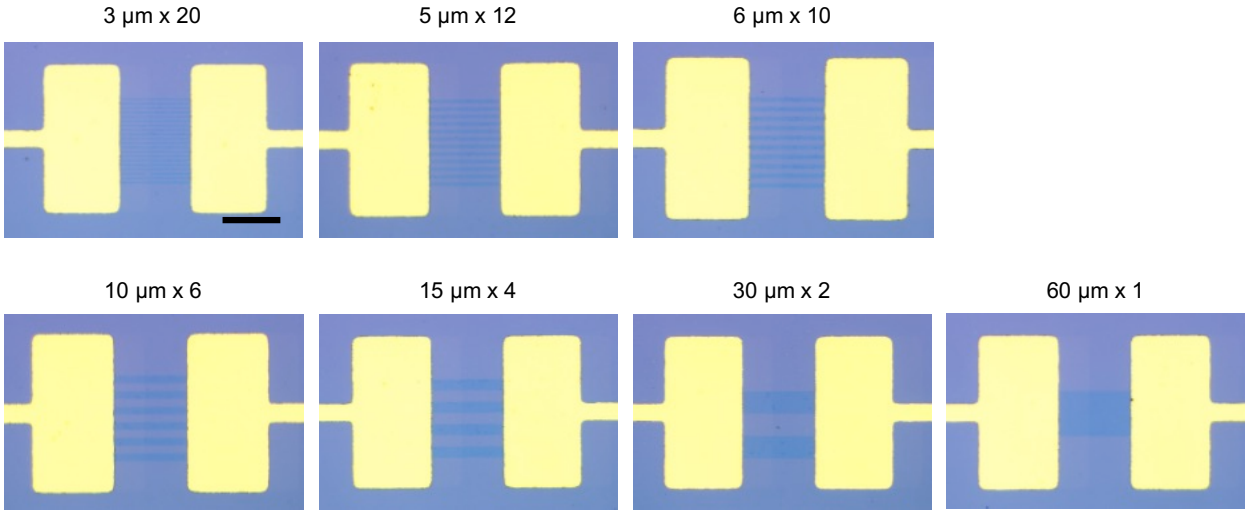

Fig. S21. Optical microscope images of graphene sensors with different edge-to-surface ratios. Scale bar, 100 µm.

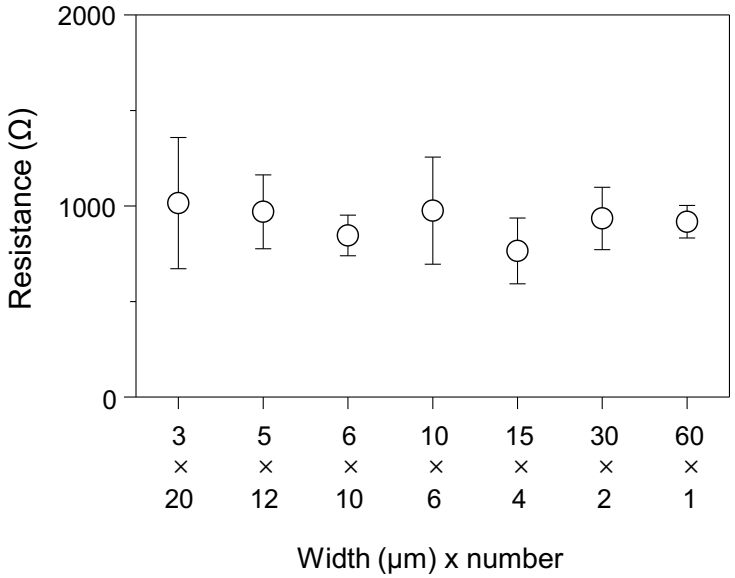

Fig. S22. Resistance vs. edge-to-surface ratio obtained before additional heat treatment in air. The resistance is uniform regardless of the edge-to-surface ratio.

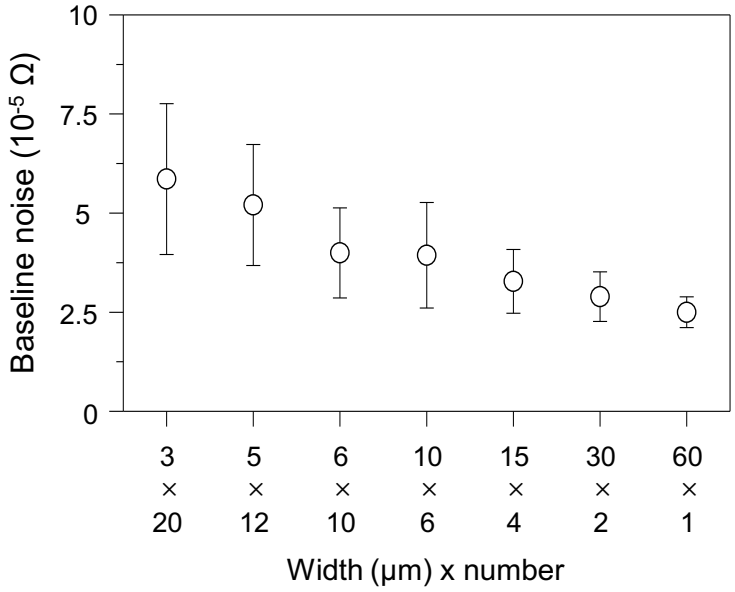

Fig. S23. Noise intensity vs. edge-to-surface ratio. Both the noise intensity and the variation of the noise increases at higher edge-to-surface ratio.

REFERENCES

(1) HyungáCheong, W.; HyebáSong, J.; JoonáKim, J., Wearable, Wireless Gas Sensors Using Highly Stretchable and Transparent Structures of Nanowires and Graphene. *Nanoscale* **2016,** *8*, 10591-10597.

(2) Kim, Y.-T.; Lee, S.; Park, S.; Lee, C. Y., Graphene Chemiresistors Modified with Functionalized Triphenylene for Highly Sensitive and Selective Detection of Dimethyl Methylphosphonate. *RSC Advances* **2019,** *9*, 33976-33980.

(3) Yoo, R.; Yoo, S.; Lee, D.; Kim, J.; Cho, S.; Lee, W., Highly Selective Detection of Dimethyl Methylphosphonate (DMMP) Using CuO Nanoparticles/ZnO Flowers Heterojunction. *Sensors and Actuators B: Chemical* **2017,** *240*, 1099-1105.

(4) Wang, Y.; Yang, M.; Liu, W.; Dong, L.; Chen, D.; Peng, C., Gas Sensors Based on Assembled Porous Graphene Multilayer Frameworks for DMMP Detection. *Journal of Materials Chemistry C* **2019,** *7*, 9248-9256.

(5) Alizadeh, T.; Soltani, L. H., Reduced Graphene Oxide-Based Gas Sensor Array for Pattern Recognition of DMMP Vapor. *Sensors and Actuators B: Chemical* **2016,** *234*, 361-370.

(6) Wang, Y.; Zhou, Z.; Yang, Z.; Chen, X.; Xu, D.; Zhang, Y., Gas Sensors Based on Deposited Single-Walled Carbon Nanotube Networks for DMMP Detection. *Nanotechnology* **2009,** *20*, 345502.

(7) Cattanach, K.; Kulkarni, R. D.; Kozlov, M.; Manohar, S. K., Flexible Carbon Nanotube Sensors for Nerve Agent Simulants. *Nanotechnology* **2006,** *17*, 4123.

(8) Wang, Y.; Yang, Z.; Hou, Z.; Xu, D.; Wei, L.; Kong, E. S.-W.; Zhang, Y., Flexible Gas Sensors with Assembled Carbon Nanotube Thin Films for DMMP Vapor Detection. *Sensors and Actuators B: Chemical* **2010,** *150*, 708-714.

(9) Wei, L.; Shi, D.; Ye, P.; Dai, Z.; Chen, H.; Chen, C.; Wang, J.; Zhang, L.; Xu, D.; Wang, Z., Hole Doping and Surface Functionalization of Single-Walled Carbon Nanotube Chemiresistive Sensors for Ultrasensitive and Highly Selective Organophosphor Vapor Detection. *Nanotechnology* **2011,** *22*, 425501.

(10) Kong, L.; Wang, J.; Luo, T.; Meng, F.; Chen, X.; Li, M.; Liu, J., Novel Pyrenehexafluoroisopropanol Derivative-Decorated Single-Walled Carbon Nanotubes for Detection of Nerve Agents by Strong Hydrogen-Bonding Interaction. *Analyst* **2010,** *135*, 368-374.

(11) Wang, F.; Gu, H.; Swager, T. M., Carbon Nanotube/Polythiophene Chemiresistive Sensors for Chemical Warfare Agents. *Journal of the American Chemical Society* **2008,** *130*, 5392-5393.

(12) Lee, J. S.; Kwon, O. S.; Park, S. J.; Park, E. Y.; You, S. A.; Yoon, H.; Jang, J., Fabrication of Ultrafine Metal-Oxide-Decorated Carbon Nanofibers for DMMP Sensor Application. *ACS Nano* **2011,** *5*, 7992-8001.

(13) Zeng, L.; Dai, C.; Liu, B.; Xue, C., Oxygen-Assisted Stabilization of Single-Atom Au During Photocatalytic Hydrogen Evolution. *Journal of Materials Chemistry A* **2019,** *7*, 24217-24221.

(14) Stadnichenko, A.; Kibis, L.; Svintsitskiy, D.; Koshcheev, S.; Boronin, A., Application of RF Discharge in Oxygen to Create Highly Oxidized Metal Layers. *Surface Engineering* **2018,** *34*, 1-5.

(15) Yamamoto, M.; Matsumae, T.; Kurashima, Y.; Takagi, H.; Suga, T.; Itoh, T.; Higurashi, E., Comparison of Argon and Oxygen Plasma Treatments for Ambient Room-Temperature Wafer-Scale Au–Au Bonding Using Ultrathin Au Films. *Micromachines* **2019,** *10*, 119.

(16) Stadnichenko, A.; Koshcheev, S.; Boronin, A., An XPS and TPD Study of Gold Oxide Films Obtained by Exposure to RF-Activated Oxygen. *Journal of Structural Chemistry* **2015,** *56*, 557-565.

(17) Juodkazis, K.; Juodkazyt, J.; Jasulaitien, V.; Lukinskas, A.; Šebeka, B., XPS Studies on the Gold Oxide Surface Layer Formation. *Electrochemistry Communications* **2000,** *2*, 503-507.